

NORTH ANATOLIAN AND EAST ANATOLIAN FAULTS BEYOND
KARLIOVA IN THE EAST

by

Müfide Elvanlı

B.S., Geomatics Engineering, Erciyes University, 2016

Submitted to the Kandilli Observatory and Earthquake
Research Institute in partial fulfillment of
the requirements for the degree of
Master of Science

Graduate Program in Geodesy

Boğaziçi University

2021

ACKNOWLEDGEMENTS

First of all, I would like to express my deepest gratitude to my supervisor Assoc. Prof. Dr. Aslı Dođru for motivation and immense guidance. Since the beginning of this study, she made me believe in myself and took my hand in every obstacle I was stuck with. She never spared her kindly help and invaluable time and generously shared her knowledge and experience with me; besides, I always felt her emotional support. I could never end up this study without her endless support. It was a great pleasure to have the opportunity to study with her.

I am warmly thankful to Assoc. Prof. Dr. Fatih Bulut for generously sharing his eye-opening knowledge and guiding my ideas with his valuable experiences. I am also grateful for the program he developed for arctangent profiling analysis, which is the key point of the study, and also for his continuous support.

Special thanks I want to give to Prof. Dr. Bahadır Aktuđ who is the member of the jury, for his time, and for sharing the ERBLOM software that helped me diversify my study with me.

I am deeply thankful to Prof. Dr. Haluk Özener and Prof. Dr. Semih Ergintav for sharing their experiences, valuable advice, and encouragement. My special thanks also to all faculty members in the KOERI, Geodesy Department, for their sincerity. I have spent precious years in this department, I am grateful to anyone who gave me the chance of studying here.

Last but not the least, I want to send my profound gratitude to my parents Ayşegül-Musa Er, since they brought me to the person I am today. They have always trusted and believed in me. I am also thankful to my hearties Eslem Sirye, Ahmet Emin and Mevanur Feyza who made my life meaningful and cheerful. My most special thanks go to my husband Olcay Elvanlı who is being with me whenever I need him. Throughout my education, he always encouraged and supported me to go one step further. I am grateful for all the strength, moral and material supports he has given me throughout my education.

ABSTRACT

NORTH ANATOLIAN AND EAST ANATOLIAN FAULTS BEYOND KARLIOVA IN THE EAST

The vicinity of Karliova, located at the intersection of two major fault systems in Turkey, is a seismically active region with a tectonically complex structure, however; there is little information about the east of Karliova, to what extent in the east the seismic activity continues. Investigating the possible extensions of the North Anatolian Fault (NAF) and the East Anatolian Fault (EAF) to the east of Karliova is therefore significant target to verify if there is a strain accumulation and therefore unknown earthquake hazard in the region. In this study, possible extensions of the NAF and the EAF in the east of Karliova were investigated using GPS slip rates. In this context, historical and instrumental period earthquakes had been compiled to identify potential indications for the possible extensions of the NAF and the EAF in the east of Karliova. With the focal mechanism solutions, it has been observed that the tectonics of this particular region is dominated by mostly strike slip structures. Fault information in previous studies conducted in the region was compiled to locate of potential eastern extensions to be used in the analysis. Also, the all-available GPS stations were homogenously combined (CORS-TR and campaign-based GPS measurements) to achieve the best possible station coverage to characterize tectonic surface deformation in the region. Using combined GPS data, Arc tangent profiling analysis and block modeling analysis were performed to determine the location and movement of the potential extensions of the NAF and the EAF. The results of the analysis have shown that there is a strike slip faulting activity in the east of Karliova suggesting continuation of the NAF and the EAF in the east. The NAF extends ~ 170 km southeast of Karliova, by the slip rate of about 10.3 mm/y. The EAF extends ~ 180 km northeast of Karliova, by the slip rate of about 5.8 mm/y. For both fault systems, slip rates drastically decrease to the east of Karliova, down to the half of their slip rates in the west.

ÖZET

KARLIOVA'NIN DOĞUSUNDA KUZEY ANADOLU VE DOĞU ANADOLU FAYLARI

Türkiye'deki iki büyük fay sisteminin kesişme noktasında yer alan Karlıova ve çevresi, karmaşık bir tektonik yapıya sahip olan, sismik olarak aktif bir bölgedir, ancak Karlıova'nın doğusunda sismik aktivitenin ne ölçüde devam ettiği hakkında çok az bilgiye sahibiz. Karlıova'nın doğusuna uzanan Kuzey Anadolu Fayı (KAF) ve Doğu Anadolu Fayı'nın (DAF) olası uzantılarının araştırılması, bölgedeki gerinim birikimini ve dolayısıyla bilinmeyen bir deprem tehlikesi olup olmadığını doğrulamak için önemli bir hedefdir. Bu çalışmada, KAF ve DAF'ın Karlıova'nın doğusundaki olası uzantıları, GPS kayma oranları kullanılarak incelenmiştir. Bu bağlamda, Karlıova'nın doğusunda KAF ve DAF'ın olası uzantılarına yönelik potansiyel göstergeleri belirlemek için tarihsel ve aletsel dönem depremleri derlenmiştir. Odak mekanizma çözümleri ile, bu bölgenin tektoniğinde çoğunlukla doğrultu atımlı yapıların hakim olduğu gözlenmiştir. Bölgede yapılan önceki çalışmalarda bulunan fay bilgileri derlenerek, analizde kullanılacak olası doğu uzantıları tespit edilmiştir. Ayrıca, bölgedeki tektonik yüzey deformasyonunu karakterize etmek için mümkün olan en iyi istasyon kapsama alanını elde etmek için mevcut tüm GPS istasyonları (CORS-TR ve kampanya bazlı GPS ölçümleri) homojen bir şekilde birleştirildi. Uzantıların konumunu ve hareketini belirlemek için birleştirilmiş GPS verileri kullanılarak arctangent profil analizi ve blok modelleme analizi gerçekleştirilmiştir. Analizlerin sonuçları, Karlıova'nın doğusunda doğrultu atımlı bir faylanma aktivitesinin olduğunu ve KAF ve DAF'ın doğuda devam ettiğini düşündürmektedir. KAF, doğuda yaklaşık 10.3 mm/y kayma hızıyla Karlıova'nın ~ 170 km güneydoğusuna uzanmaktadır. DAF ise, doğuda yaklaşık 5.8 mm/y kayma hızıyla Karlıova'nın ~ 180 km kuzeydoğusuna uzanmaktadır. Her iki fay sistemi için, Karlıova'nın doğusuna doğru kayma hızları, batıdaki kayma hızlarının yarısına kadar, büyük ölçüde azalmaktadır.

TABLE OF CONTENTS

ACKNOWLEDGEMENTS.....	iii
ABSTRACT.....	iv
ÖZET	v
LIST OF FIGURES	vii
LIST OF TABLES.....	ix
LIST OF SYMBOLS	x
LIST OF ACRONYMS/ABBREVIATIONS.....	xi
1. INTRODUCTION	1
2. TECTONIC SETTINGS OF EASTERN ANATOLIA	4
2.1. Study Area.....	4
2.2. Present Day and Historical Seismicity.....	7
2.2. Focal Mechanisms.....	13
3. METHODOLOGY AND DATA SET	14
3.1. Combining Velocity Fields	13
3.2. Combining Faults	13
4. ANALYSIS AND RESULTS.....	17
4.1. Arctangent Profiling.....	13
4.2. Block Modeling.....	27
5. DISCUSSION.....	29
6. CONCLUSION	32
REFERENCES	34

LIST OF FIGURES

Figure 1.	The basic tectonic map of Turkey with earthquakes occurred between 1900-2021. Black arrows show the relative movement of plates. The area inside the purple rectangle is the studying area. The green point indicates the location of Karlioiva. Map was created using the data from Bulut et al. (2012), and earthquake data taken from KOERI.	2
Figure 2.1.	Tectonic setting of the study area. Abbreviations, HSF, KF, KS, ES, AGF, HGF, SF, KMF mean Horasan Senkaya fault, Karayazi fault, Kargapazari segment, Elmali segment, Akdogan Golu fault, Hasantimur Golu fault, Surgu fault and Kahramanmaras fault, respectively. Data of faults shown in black were taken from MTA. Data of faults and segments shown in red were taken from Emre et al. (2018).	7
Figure 2.2.1.	Historical seismicity of the study area. In cases where more than two earthquakes occurred at the same location, only the date of one is shown (please see Table 2.2 for details).....	9
Figure 2.2.2.	Present day seismicity of the study area.	10
Figure 2.3.	Focal mechanism solutions. Data were taken from ISC.	13
Figure 3.1.	GPS velocity field of the region in the ITRF08 reference frame. Data from Kreemer et al. (2014) are shown with red arrows, data from Ozdemir (2016) are shown with blue arrows and data from Aktug et al. (2016) are shown with green arrows.	15
Figure 3.2.	Faults from previous studies within the study area. The faded lines were taken from the MTA.....	16

- Figure 4.1.1. Arctangent analysis of the NAF section. In upper panel, the location of the fault used for the best fit solution is shown with a green “X” sign in the lower panel, and the region where the profile was taken..... 19
- Figure 4.1.2. Arctangent analysis of the southeast extension of the NAF section. In the upper panel, the location of the marked fault used for the best fit solution is shown with a green “X” sign in the lower panel, and the region where the profile was taken.21
- Figure 4.1.3. Arctangent analysis of the easternmost extension of the NAF section. In the upper panel, the location of the marked fault used for the best fit solution is shown with a green “X” sign in the lower panel, and the region where the profile was taken.....22
- Figure 4.1.4. Arctangent analysis of the EAF section. In the upper panel, the location of the marked fault used for the best fit solution is shown with a green “X” sign in the lower panel, and the region where the profile was taken.24
- Figure 4.1.5. Arctangent analysis of the extension of the EAF section. In the upper panel, the location of the marked fault used for the best fit solution is shown with a green “X” sign in the lower panel, and the region where the profile was taken.26
- Figure 4.2. Block modeling analysis of the study and the block boundaries indicated with the yellow lines. The faded lines were taken from the MTA, and the white colored faults were taken from previous studies. GPS velocity vectors represent the red ones from Kreemer et al. (2014), the blue ones from Aktug et al. (2016), and the green ones from Ozdemir (2016).28

LIST OF TABLES

Table 2.2.	List of historical earthquakes that occurred in the study area.	11
Table 4.1.	Slip rates and locking depths from arctangent analysis. Abbreviations, SR, LD mean slip rate and locking depth, respectively.	27
Table 4.2.	Slip rates from block modeling analysis.	28

LIST OF SYMBOLS

D	Locking Depth
M	Magnitude
M _w	Moment Magnitude
V	Far Field Velocity
V _x	Velocity of Points
x	Distance from the Fault

LIST OF ACRONYMS/ABBREVIATIONS

AGF	Akdogan Golu Fault
CORS-TR	Continuously Operating Reference Stations - Turkey
DAF	Doğu Anadolu Fayı
E	East
EAF	East Anatolian Fault
ERBLOM	Elastic Rigid Block Modeling
ES	Elmalı Segment
F	Fault
GPS	Global Positioning System
HGF	Hasantimur Golu Fault
HSF	Horasan Senkaya Fault
ISC	International Seismology Centre
ITRF	International Terrestrial Reference Frame
KAF	Kuzey Anadolu Fayı
KF	Karayazi Fault
km	Kilometer
KMF	Kahramanmaras Fault
KS	Kargapazari Segment
KOERI	Kandilli Observatory and Earthquake Research Institute
LD	Locking Depth
mm	Millimeter
MTA	Maden Teknik ve Arama Genel Müdürlüğü / General Directorate of Mineral Research and Exploration
N	North
NAF	North Anatolian Fault
S	Segment
SF	Surgu Fault
SR	Slip Rate
y	Year

1. INTRODUCTION

The earthquakes produced by the steady-stated motion of the earth's tectonic plates cause many losses in human life. Based on the earthquakes that have already caused fatal losses in the past, it is indispensable to characterize seismically active faults that has a potential to generate large earthquakes in future. Turkey accommodates two seismically active major transform fault systems, namely the East Anatolian Fault (EAF) and the North Anatolian Fault (NAF). The NAF is a dextral fault system, extending for ~1200 km from the North Aegean Sea in the west towards Karliova in the east (Sengor, 1979; Sengor and Canitez 1982; McClusky et al., 2000). The EAF is a southwest northeast striking sinistral fault system, extending for ~560 km from Kahramanmaras triple junction in the southwest, towards Karliova in the northwest (McKenzie, 1976; Taymaz et al., 1991; Bulut et al., 2012). As described above, these fault systems conjugate in Karliova. (Figure 1)

These two main fault systems deform two plate boundaries at 10+ mm/y slip rates and therefore have high potential to generate destructive earthquakes. Based on the historical and instrumental period earthquake records, the NAF has generated 40 M7+ earthquakes since 29 CE. The EAF, which has almost a half deformation rate compared to the NAF, has generated 15 M7+ earthquakes since 69 BC. For this reason, it is of great importance to forecast the location and the magnitude of future earthquakes that may occur on these faults in order to determine the earthquake hazard and therefore the risks in the region. In this context, there are various earth science studies conducted to investigate these fault systems. These studies are carried out to understand the kinematic characteristics, inter-seismic deformation, and complete failure of these fault systems in order to minimize the damages they might cause generating large earthquakes.

According to the results obtained from previous studies, the slip rate of the NAF in the west of Karliova is ~20 mm/y (Aktug et al., 2015), and the slip rate of the EAF between Karliova and Kahramanmaras junction is about 10 mm/y (Aktug et al., 2016). However, there is only a little known how the Earth's crust deforms along the eastward possible extensions of these faults in the east of Karliova.

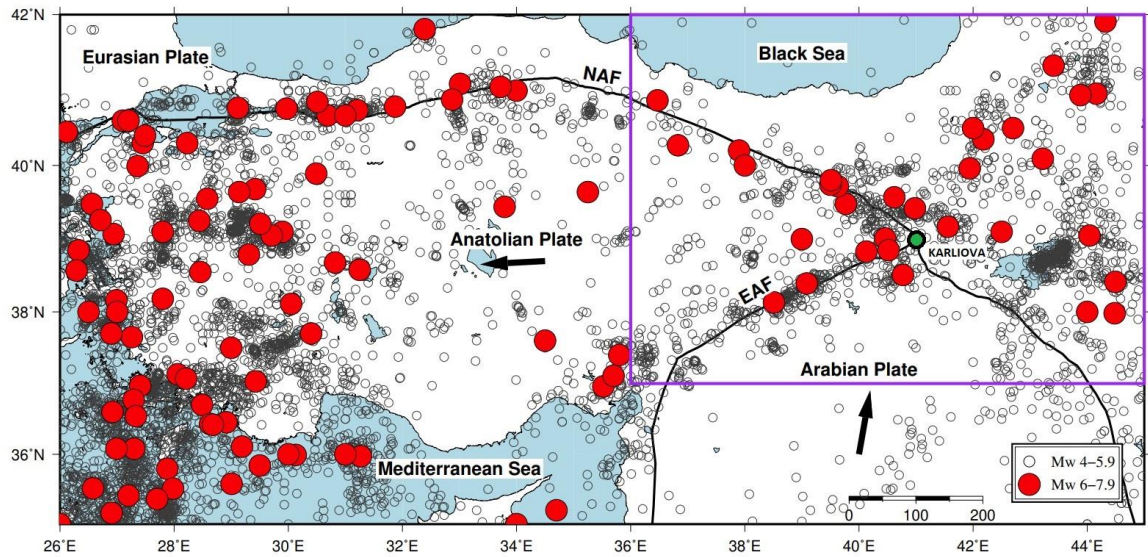


Figure 1. The basic tectonic map of Turkey with earthquakes occurred between 1900-2021. Black arrows show the relative movement of plates. The area inside the purple rectangle is the studying area. The green point indicates the location of Karliova. Map was created using the data from Bulut et al. (2012), and earthquake data taken from KOERI.

Future major earthquakes can be forecasted on a fault segment, its earthquake generation cycle, interseismic slip rate and coupling are sufficiently known. Slip rates and coupling can be investigated using GPS data if sufficient GPS data are available. Another challenge is to precisely locate the faults that might produce earthquakes, especially, in the cases where no active fault is reported. In this frame, arctangent modeling of GPS measurements is a straightforward tool to simultaneously determine locations of seismically active faults, their slip rates and couplings, in other words, locking depths.

In this study, we investigated whether the NAF and the EAF continue deforming eastward beyond the east of Karliova. As Karliova region host an intersection of two major transform faults, it has a complicated structural setting including secondary faults in addition to the major faults. In this region, bridging the earthquakes and the associated faults is indispensable to characterize the earthquake hazard. This requires locations of the faults, their latest failure, dimensions, kinematics, slip rates and locking depths to forecast how large the earthquakes might generate, and therefore mitigate their potential damage.

There are only few studies conducted on the possible extensions of the NAF and the EAF in the east of Karlova. In most of these studies, the extension of the NAF, the Varto fault, has been investigated. Philip et al. (1989) and Rebai et al. (1993) reported that there is a distinct fault northeast of Karlova. Philip et al. (2001) showed that the fault trace is a continuation of the EAF. Additionally, the fault traces therein roughly characterize continuations of the NAF and the EAF by Karakhanian et al. (2004). Among these investigations, there is not yet a study reporting their slip rates. To fill this gap, this thesis aims to contribute to better understanding tectonic slip rates of the NAF, and EAF, and their possible extensions in the east, which will lead to better assessment of earthquake hazard in this target region.

In the first step, the historical and the instrumental period earthquakes and their focal mechanisms were compiled to identify earthquake-generating faults in the region. In a second step, previous structural investigations were reviewed to compile all known seismically active faults in the region. In a next step, all available GPS velocity data were combined to have the best possible coverage of GPS slip rates. Finally, fault-perpendicular arcant profiles of GPS velocities were investigated across the NAF, the EAF, and their possible extensions in the east of Karlova. Additionally, an elastic block modeling was performed to further constrain slip rates in this intersection zone based on homogenously combined GPS velocity field using ERBLOM software (Aktug et al., 2013, Aktug et al., 2015)

2. TECTONIC SETTINGS OF EASTERN ANATOLIA

2.1 Study Area

The study area is located in eastern Turkey remaining between the latitudes of 37N-42N and the longitudes of 36E-45E. The importance of the region is that it is tectonically complex and has a high earthquake potential as it accommodates an intersection between two major transform faults. It covers the area east of the NAF and the northeast of the EAF, the Karlioiva region where they intersect, and a region to the east where we investigate their potential eastward continuations. There are many tectonically active structures in this region in addition to the NAF and the EAF.

The most active tectonic structure in the study area is the dextral NAF. Its segments near Karlioiva have different lengths with slightly different kinematics. The 90 km long Resadiye segment is the westernmost segment of the NAF in the study area. The Susehri segment is located just in the east of the Resadiye segment extending 65 km. The Refahiye segment has a length of 49 km following the Susehri segment eastward. The 42 km long Erzincan segment operates through a sedimentary basin in a close vicinity to Erzincan city center. The 77 km long Yedisu segment extends from the eastern tip of the Erzincan segment to the western tip of Elmali segment. The Elmali segment extends between the Yedisu and the Kargapazari segments for 22 km. The Kargapazari segment is the easternmost segment of the NAF in the study area, extending for 39 km. (Emre et al., 2018) (Figure 2.1)

The second most active tectonic structure in the study area is the sinistral EAF. Its segments near Karlioiva have different lengths with slightly different kinematics than the overall sinistral behavior of the EAF. The Karlioiva segment represents the north-easternmost segment of the EAF starting from its intersection with the NAF towards the southwest extending for 31 km. The Ilica segment is 37 km from the southwestern tip of the Karlioiva segment towards northeastern tip of the Palu segment near Bingol city. The Palu segment starts near Bingol city center and extends to the Puturge segment extending for 77 km. The 97 km long Puturge segment extends between the Palu segment and the Erkenek segments.

The Erkenek segment follows the Puturge segment in the southwest extending for 77 km. The Pazarcik segment is the south-westernmost segment of the EAF in the study area, extending for 82 km long. (Emre et al., 2018) (Figure 2.1)

In addition to the NAF and the EAF, there are also individual fault segments in the study area. About 20 of them are considered in this study. These are shown in Figure 2.1. These faults segments are also described below following Emre et al. (2018):

- (i) The Deliler fault is a NE-SW striking 204 km long sinistral fault located in the central Anatolia.
- (ii) The Divrigi fault is an E-W striking 69 km long reverse fault follows the Deliler fault to the northeast.
- (iii) The Sariz fault is a NE-SW striking 215 km long sinistral fault.
- (iv) The Savrun fault is a NE-SW striking 60 km long sinistral fault located in the northwest of Kahramanmaras city center.
- (v) The Kahramanmaras fault is an E-W striking 42 km long reverse fault and adjacent to the Savrun fault.
- (vi) The Surgu fault connects the EAF and the Malatya fault. It is an E-W striking sinistral fault with 79 km.
- (vii) The Malatya fault is a N-S striking 176 km long sinistral fault line passing through the west of Malatya city.
- (viii) The Ovacik fault is located between the NAF and the Malatya fault. It is a NE-SW striking 136 km long sinistral fault.
- (ix) The Varto fault starts at Karliova junction where the EAF and the NAF intersect and continues 45 km eastward. It is a NW-SE striking dextral fault.
- (x) The Akdogan Golu fault is an E-W striking 47 km long dextral fault located just east of the Varto fault.
- (xi) The 92 km long Erzurum fault passes from near the Erzurum city center. General structure is NE-SW striking sinistral fault.
- (xii) The NW-SE striking 59 km long, dextral, Karayazi fault runs parallel to the Varto fault in the east of Erzurum.
- (xiii) The Tutak fault follows the Karayazi fault towards the east. It is a NW-SE striking 57 km long dextral fault.

- (xiv) The Horasan Senkaya fault is located in northeast of Erzurum fault, with NE-SW striking 56 km long. It includes sinistral and reverse fault structures.
- (xv) The Gole fault is NE-SW striking 33 km long sinistral fault and located in the far northeast of Turkey.
- (xvi) The Ercis fault is a NW-SE striking 59 km long dextral structure that passes northeast of the Van Lake.
- (xvii) The Van fault is an E-W striking 27 km long reverse fault adjacent the Van Lake.
- (xviii) The Caldıran fault is one of the fault fractures in the far east of Turkey for 52 km. It is a NW-SE striking dextral fault.
- (xix) The Hasantimur Golu fault is a NW-SE striking 32 km long dextral fault.
- (xx) Saray fault which has a NW-SE striking dextral structure is located in the easternmost part of Turkey, with 24 km long.

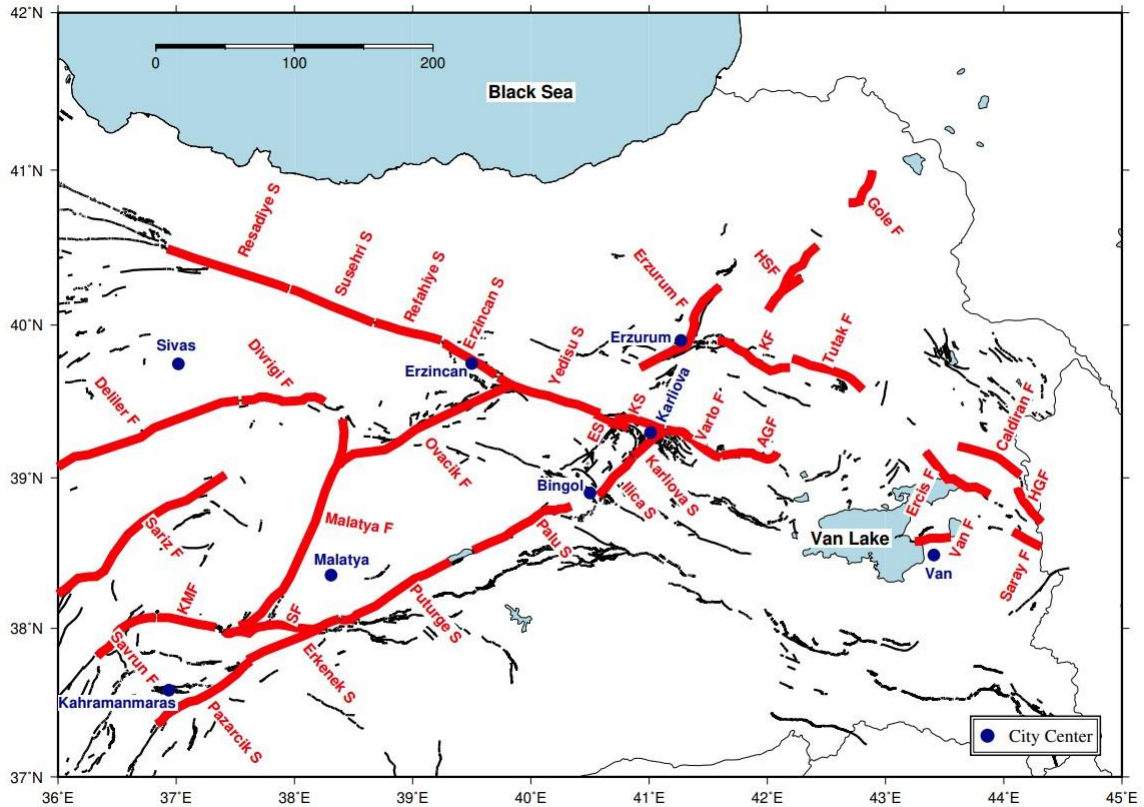


Figure 2.1. Tectonic setting of the study area. Abbreviations, HSF, KF, KS, ES, AGF, HGF, SF, KMF mean Horasan Senkaya fault, Karayazi fault, Kargapazari segment, Elmali segment, Akdogan Golu fault, Hasantimur Golu fault, Surgu fault and Kahramanmaras fault, respectively. Data of faults shown in black were taken from MTA. Data of faults and segments shown in red were taken from Emre et al. (2018).

2.2. Present Day and Historical Seismicity

Historical and instrumental period earthquakes that occurred in the region were examined to identify seismically active faults in the region. Bornhoff et al. (2016), Ambraseys and Jackson (1998), and the KOERI database were used to compile destructive historical earthquakes that occurred before 1900 CE. Totally, 73 seismic events were available in the study area that recorded for the time period of 75 - 1900 CE within the magnitude range of 6 - 8. In the historical period, few severe earthquakes occurred in the vicinity of Karliova to the east (Table 2.2, Figure 2.2.1)

The instrumental period earthquakes after 1900 CE were obtained from the KOERI earthquake catalogue. Totally 115 devastating earthquakes occurred along fault systems in the study area. 96 of them are in the magnitude range of 6 - 7. 19 of them are in the magnitude range of 7 - 8. Figure 2.2.2 shows the present-day earthquakes regarding their locations and magnitudes.

In both cases, epicenters of M6+ earthquakes do not characterize straight lines as continuations of the NAF or the EAF in the southeast or in the northeast of Karlıova. However, overall distributions of the epicenters suggest a similar trend for broad zones. In historical earthquake catalog, the 1866, the 1685, the 75, the 1582, and the 602 earthquakes suggest a northwest-southeast striking epicentral zone in the southeast of Karlıova (Figure 2.2.1). Similarly, the 1852, the 1859, the 1688, the 1718, and the 1766 earthquakes suggest a southwest-northeast striking epicentral zone in the southeast of Karlıova (Figure 2.2.1). In instrumental period earthquake catalog, epicenters in the southeast of Karlıova indicate a clear continuation of the NAF with a similar strike towards the Van Lake (Figure 2.2.2). They also suggest a continuation of the EAF in the northeast of Karlıova with a similar strike but covering a broader fracture zone (Figure 2.2.2).

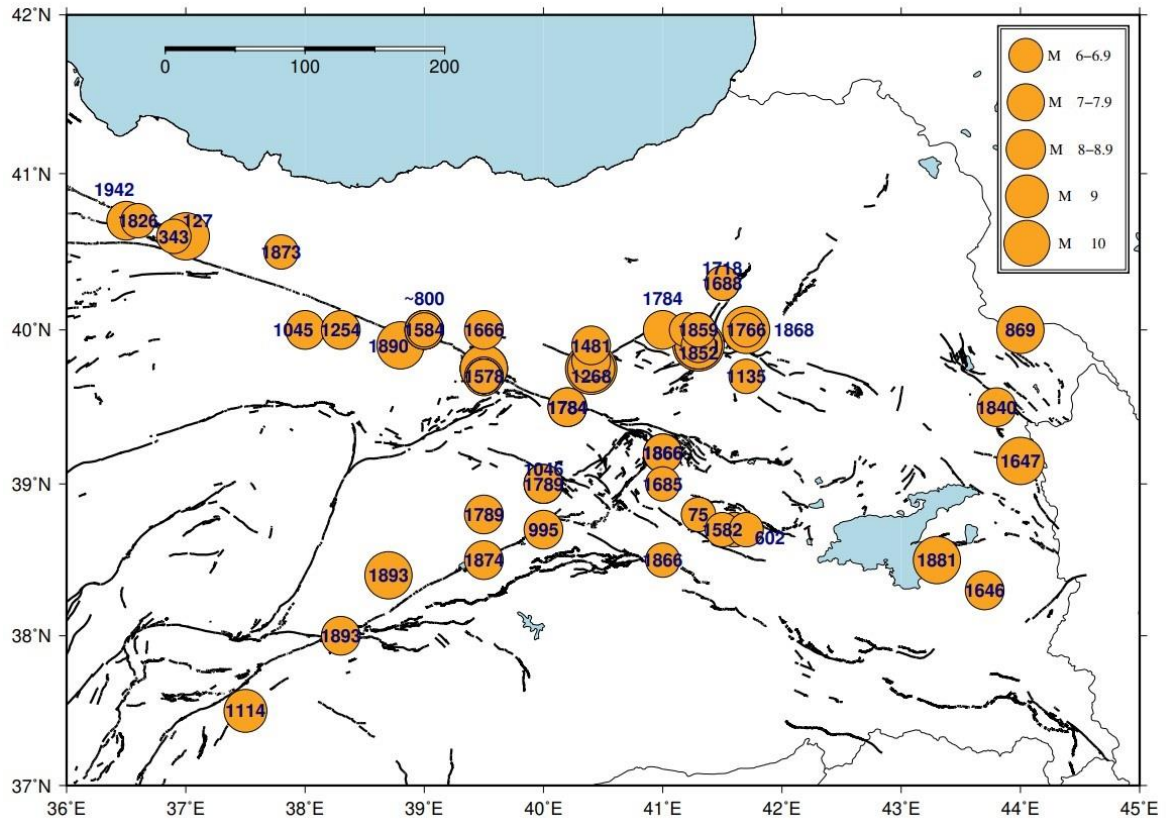


Figure 2.2.1. Historical seismicity of the study area. In cases where more than two earthquakes occurred at the same location, only the date of one is shown (please see Table 2.2 for details).

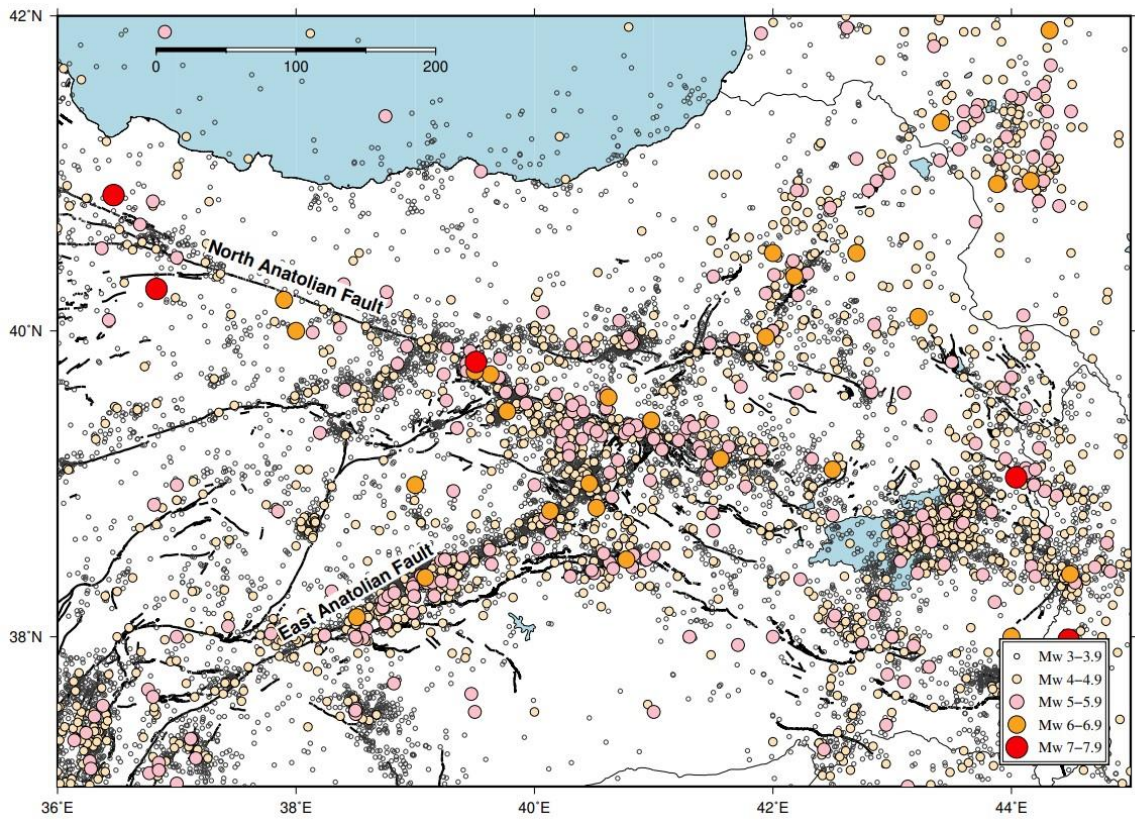


Figure 2.2.2. Present day (between 1900 CE – 2021 CE) seismicity of the study area.

Table 2.2. List of historical earthquakes that occurred in the study area.

Year	Latitude	Longitude	Magnitude	Reference
75	38.8	41.3	6.5	Bohnhoff et al. (2016)
115	35.8	36.3	$7.0 \leq M < 7.8$	Ambraseys and Jackson (1998)
127	40.6	37.0	9	KOERI
343	40.6	36.9	6.9	Bohnhoff et al. (2016)
602	38.7	41.6	6.0	Bohnhoff et al. (2016)
~800	40.0	39.0	7.5	Bohnhoff et al. (2016)
802	39.7	39.5	6.5	Bohnhoff et al. (2016)
869	40.0	44.0	9	KOERI
995	39.0	40.0	7.0	Bohnhoff et al. (2016)
995	38.7	40.0	$7.0 \leq M < 7.8$	Ambraseys and Jackson (1998)
968	41.15	34.75	9	KOERI
1011	39.7	39.5	6.5	Bohnhoff et al. (2016)
1045	40.0	38.0	$7.0 \leq M < 7.8$	Ambraseys and Jackson (1998)
1045	39.75	39.5	9	KOERI
1046	39.0	40.0	7.8	Bohnhoff et al. (2016)
1114	37.5	37.5	$M \geq 7.8$	Ambraseys and Jackson (1998)
1135	39.7	41.7	6.4	Bohnhoff et al. (2016)
1165	39.7	39.5	6.4	Bohnhoff et al. (2016)
1168	39.7	39.5	6.7	Bohnhoff et al. (2016)
1170	39.7	39.5	6.7	Bohnhoff et al. (2016)
1236	39.7	39.5	6.2	Bohnhoff et al. (2016)
1254	40.0	38.3	7.2	Bohnhoff et al. (2016)
1254	39.7	39.5	7.5	Bohnhoff et al. (2016)
1254	40.0	39.0	$7.0 \leq M < 7.8$	Ambraseys and Jackson (1998)
1268	39.8	40.4	7.4	Bohnhoff et al. (2016)
1268	39.75	40.4	9	KOERI
1308	39.7	39.5	6.5	Bohnhoff et al. (2016)
1363	38.7	41.6	6.9	Bohnhoff et al. (2016)
1422	39.7	39.5	6.7	Bohnhoff et al. (2016)
1457	39.7	39.5	6.9	Bohnhoff et al. (2016)
1458	39.75	40.4	10	KOERI
1481	39.9	40.4	7.7	Bohnhoff et al. (2016)
1482	39.75	39.5	9	KOERI
1543	39.7	39.5	6.5	Bohnhoff et al. (2016)
1578	39.7	39.5	6.5	Bohnhoff et al. (2016)
1582	38.7	41.5	6.5	Bohnhoff et al. (2016)

Table 2.2. List of historical earthquakes that occurred in the study area. (cont.)

Year	Latitude	Longitude	Magnitude	Reference
1584	40.0	39.0	6.6	Bohnhoff et al. (2016)
1584	39.75	39.5	9	KOERI
1646	38.3	43.7	7.0≤M<7.8	Ambraseys and Jackson (1998)
1647	39.15	44.0	9	KOERI
1660	40.0	41.3	6.5	Bohnhoff et al. (2016)
1660	40.0	41.2	6.5	Bohnhoff et al. (2016)
1666	40.0	39.5	7.5	Bohnhoff et al. (2016)
1668	40.9	36.0	9	KOERI
1685	39.0	41.0	6.7	Bohnhoff et al. (2016)
1688	40.3	41.5	6.5	Bohnhoff et al. (2016)
1705	38.7	41.7	6.7	Bohnhoff et al. (2016)
1718	40.3	41.5	6.5	Bohnhoff et al. (2016)
1766	40.0	41.7	6.5	Bohnhoff et al. (2016)
1784	40.0	41.0	7.1	Bohnhoff et al. (2016)
1784	39.5	40.2	7.6	Bohnhoff et al. (2016)
1784	39.5	40.2	7.6	Ambraseys and Jackson (1998)
1789	39.0	40.0	7.0	Bohnhoff et al. (2016)
1789	38.8	39.5	7.0≤M<7.8	Ambraseys and Jackson (1998)
1826	40.7	36.6	6.5	Bohnhoff et al. (2016)
1840	39.5	43.8	7.3	Ambraseys and Jackson (1998)
1852	39.9	41.3	6.0	Bohnhoff et al. (2016)
1852	39.9	41.3	9	KOERI
1859	40.0	41.3	6.5	Bohnhoff et al. (2016)
1859	39.9	41.3	9	KOERI
1866	38.5	41.0	6.8	Bohnhoff et al. (2016)
1866	39.2	41.0	7.2	Bohnhoff et al. (2016)
1866	39.2	41.0	7.2	Ambraseys and Jackson (1998)
1868	40.0	41.7	9	KOERI
1873	40.5	37.8	6.5	Bohnhoff et al. (2016)
1874	38.5	39.5	7.1	Ambraseys and Jackson (1998)
1875	38.5	39.5	6.7	Ambraseys and Jackson (1998)
1875	39.9	41.3	10	KOERI
1881	38.5	43.3	9	KOERI
1890	40.0	39.0	7.3	Bohnhoff et al. (2016)
1890	39.9	38.8	9	KOERI
1893	38.0	38.3	7.1	Ambraseys and Jackson (1998)
1893	38.4	38.7	9	KOERI

2.3.Focal Mechanisms

The fault plane solutions obtained from ISC locally confirms dextral mechanism of the NAF as well as lateral mechanism of the EAF. These are generally in good correlation with the kinematics of the faults in the region suggested by Emre et al. (2018). In the southeast of Karlova, dextral mechanisms aligned along a NW-SE strike seems extending the NAF towards the Van Lake with prominently observed right lateral strike slip focal mechanisms. In the northeast of Karlova, sinistral mechanisms aligned along a NE-SW strike represent extension of the NAF towards the north-east with prominently observed left lateral strike slip focal mechanisms.

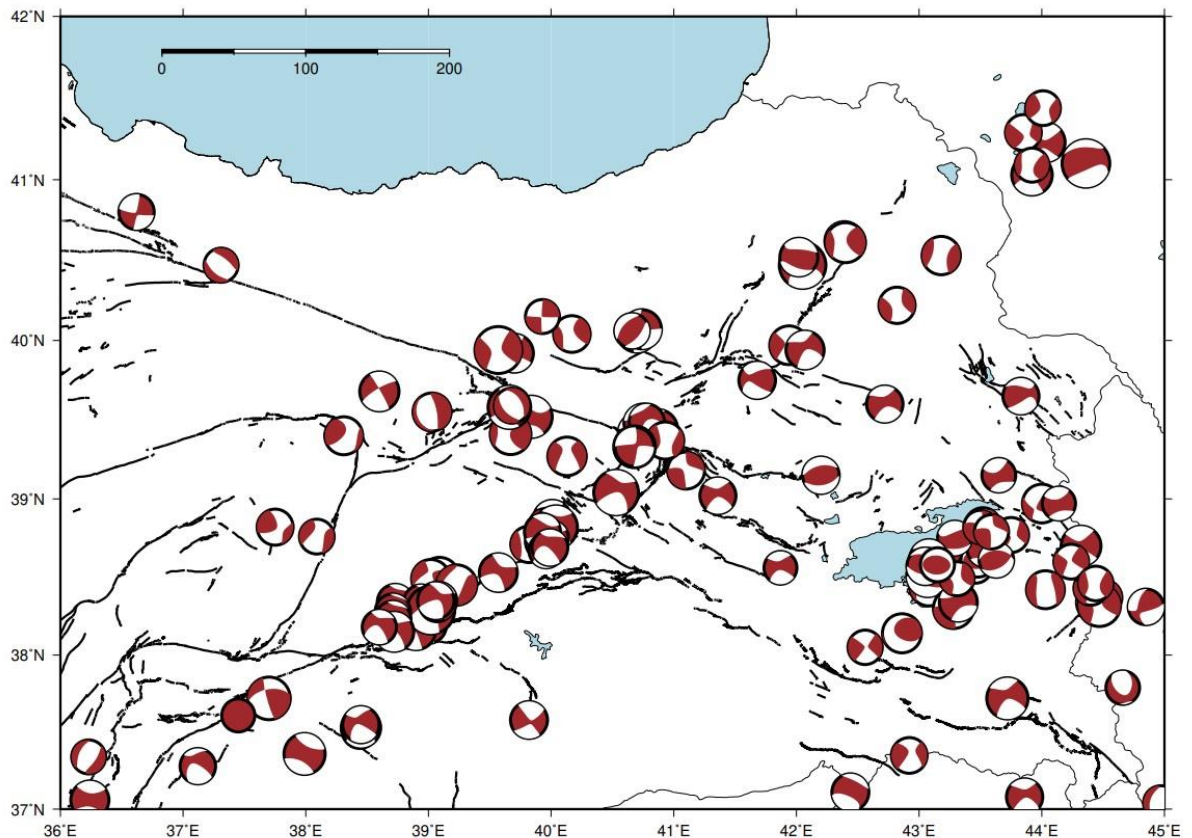


Figure 2.3. Focal mechanism solutions. Data were taken from ISC.

3. METHODOLOGY AND DATA SET

3.1. Combining Velocity Fields

Within the scope of this study, we use GPS slip rates to verify seismically active faults based on the tectonic movements at their surrounding crustal blocks. In this frame, we combined all available permanent (CORS-TR) and campaign-based GPS measurements to achieve the best available station coverage in the target region. In addition to CORS-TR (Ozdemir, 2016), we compiled GPS velocity data from Kreemer et al. (2014) and Aktug et al. (2016). In the first step, all GPS data are transformed to the same reference system (ITRF08). In a second step, overlapping and duplicated data were eliminated based on their errors. Totally, we achieved spatial coverage of 229 GPS stations, 148 from Kreemer et al. (2014), 15 from Aktug et al. (2016) and 66 from Ozdemir (2016). Combining them homogeneously, they were made ready for arctangent analysis that we perform to locate seismically active faults and to determine their slip rates as well as locking depths.

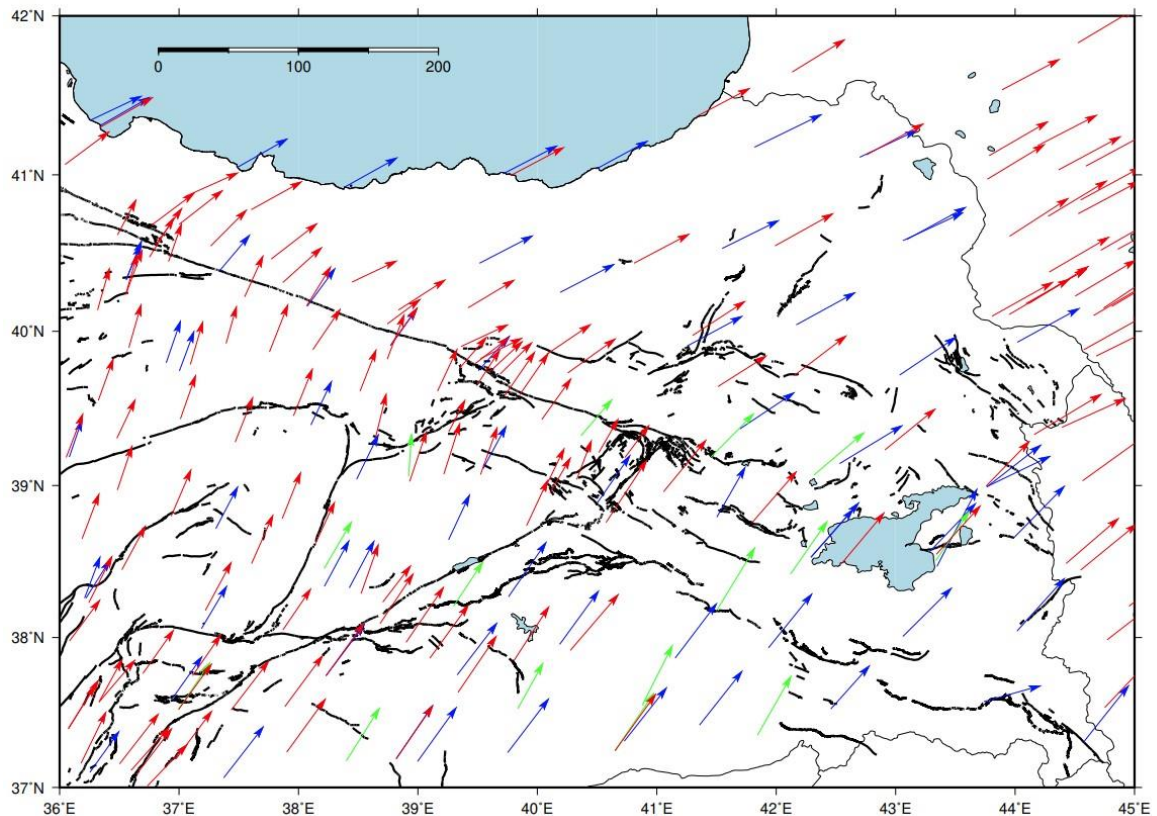


Figure 3.1. GPS velocity field of the region in the ITRF08 reference frame. Data from Kremer et al. (2014) are shown with red arrows, data from Ozdemir (2016) are shown with blue arrows and data from Aktug et al. (2016) are shown with green arrows.

3.2. Combining Faults

In order to better understand the tectonic structures in the vicinity of Karliova, previous studies in this region were carefully reviewed. Specifically, previous studies, which have focused on the eastern extensions of NAF and EAF, are the source of our review. Muehlberger and Gordon (1987) and Arpat and Saroglu (1972) verified the intersection of EAF and NAF in Karliova. Imamoglu and Cetin (2007), Karakhanian et al. (2004), McKenzie (2007), Perincek et al. (1987), Philip et al. (2001), Sengor et al. (1985) and Taymaz et al. (1990) argued that the NAF has an extension in the east beyond Karliova. Additionally, Karakhanian et al. (2004) and Philip et al. (2001) argued the idea that there is an extension of the EAF in the north of Karliova. However, as the fault maps by Karakhanian et al. (2004) and McKenzie (2007) are in low resolution, they were not included in the

combined fault map of this study. Based on all of these studies, a base fault map has been generated to investigate the tectonic slip rates they accommodate as well as their possible extensions based on GPS measurements.

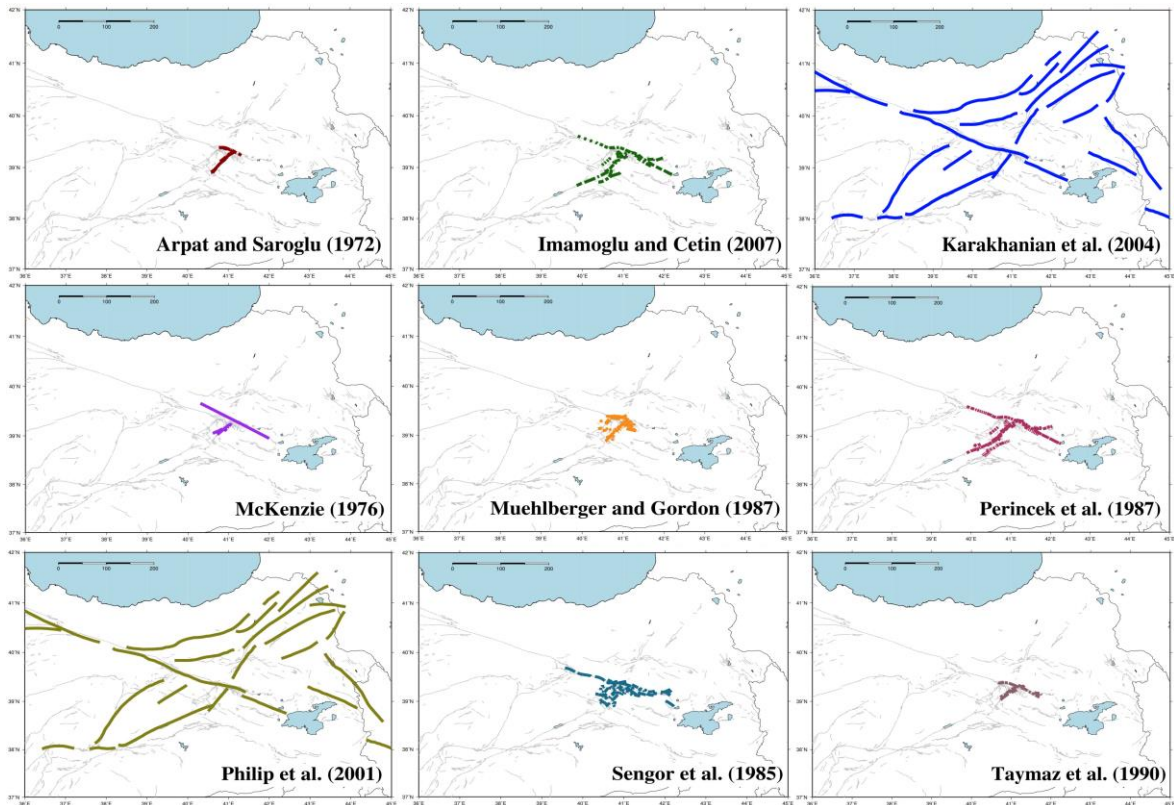


Figure 3.2. Faults from previous studies within the study area. The faded lines were taken from the MTA.

4. ANALYSIS AND RESULTS

4.1. Arctangent Profiling

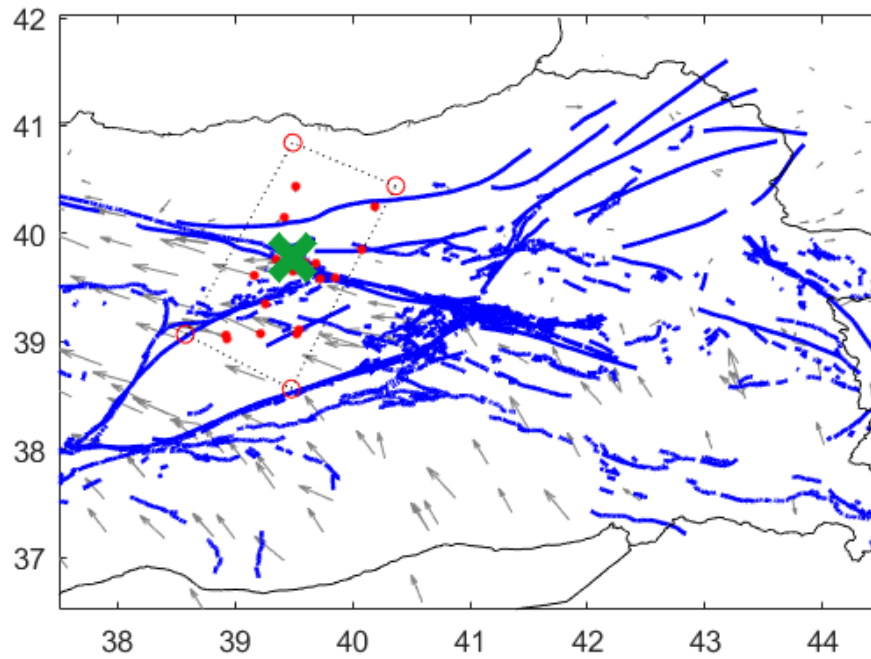
During the interseismic period, the blocks on both sides of the fault continue to slide relative to each other with small movements. In faults with a strike slip structure, while there is relatively less slip near the fault, there is an increasing movement away from the fault line. This movement in the blocks creates a shape similar to the letter S, suitable for arctangent modeling. The model of this kind of elastic deformation for strike slip faults is proposed by Savage and Burford (1973) and can be described as below:

$$V_x = \left(\frac{V}{\pi} \right) \tan^{-1} \left(\frac{x}{D} \right) \quad (4.1)$$

In the equation (4.1), where V_x is the velocity of points estimated along the perpendicular profile across the fault, V is the far field velocity, x is the distance from the fault, and D represents the locking depth.

The study area was subdivided into 5 sections as the NAF, possible southeastern extension of the NAF, possible eastern extension of the NAF and the EAF, and possible northeastern extension of the EAF to locate seismically active faults using arctangent profiling. Reference frame was fixed separately for each profile, starting from the selected reference frame, going across the fault considering availability of GPS measurements as well as the location of known seismically active faults. The analysis scheme we used, which has been developed by Bulut and Dogru, (2021), (1) plots GPS slip rates on map view, (2) marks the reference frame as a closed polygon, (3) removes the mean velocity of the selected reference frame from the entire GPS velocity field, (4) marks the edges of the arctangent profile, (5) marks the location of the fault and the mean velocity on velocity versus across-fault distance plot, (6) run a grid search to obtain the best fitting arctangent curve to optimize slip rate and locking depth, (7) resample the data 100 times randomly in the range of misfits to calculate uncertainties using bootstrap technique.

In the NAF section, reference frame was fixed at the north of the fault, basically at Eurasian plate, and across-fault profile was taken approximately 180 km long framing the NAF in the middle. Marked mean velocity and fault location are shown with green “X” marker (Figure 4.1.1). The slip rate was found to be 19.8 mm/year with an error margin of 0.8 mm/year, and the locking depth as 19.3 km with an error margin of 1.7 km.



sliprate: 19.8 ± 0.8 mm/y, locking depth: 19.3 ± 1.7 km

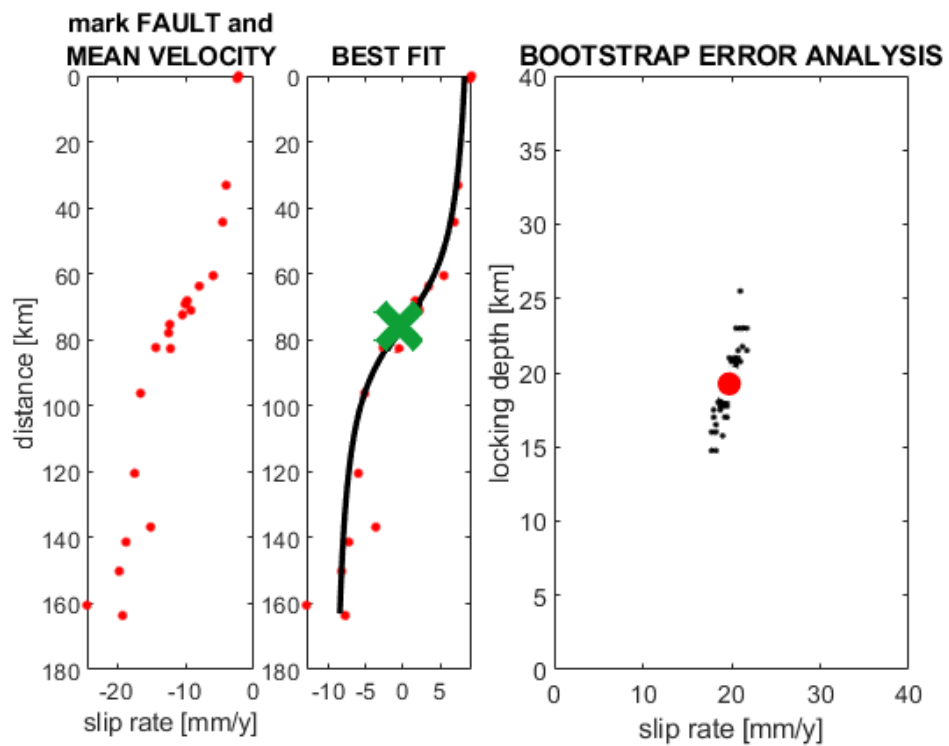


Figure 4.1.1. Arctangent analysis of the NAF section. In upper panel, the location of the fault used for the best fit solution is shown with a green “X” marker in the lower panel, and the region where the profile was taken.

In the possible southeast extension of the NAF section, reference frame was again fixed in the north of the fault, and across-fault profile was taken approximately 200 km long, which frames possible extension of the NAF in the middle. Marked mean velocity and fault location are shown with green “X” marker (Figure 4.1.2). The slip rate was found to be 10.3 mm/year with an error margin of 1.1 mm/year, and the locking depth as 9.5 km with an error margin of 2.8 km.

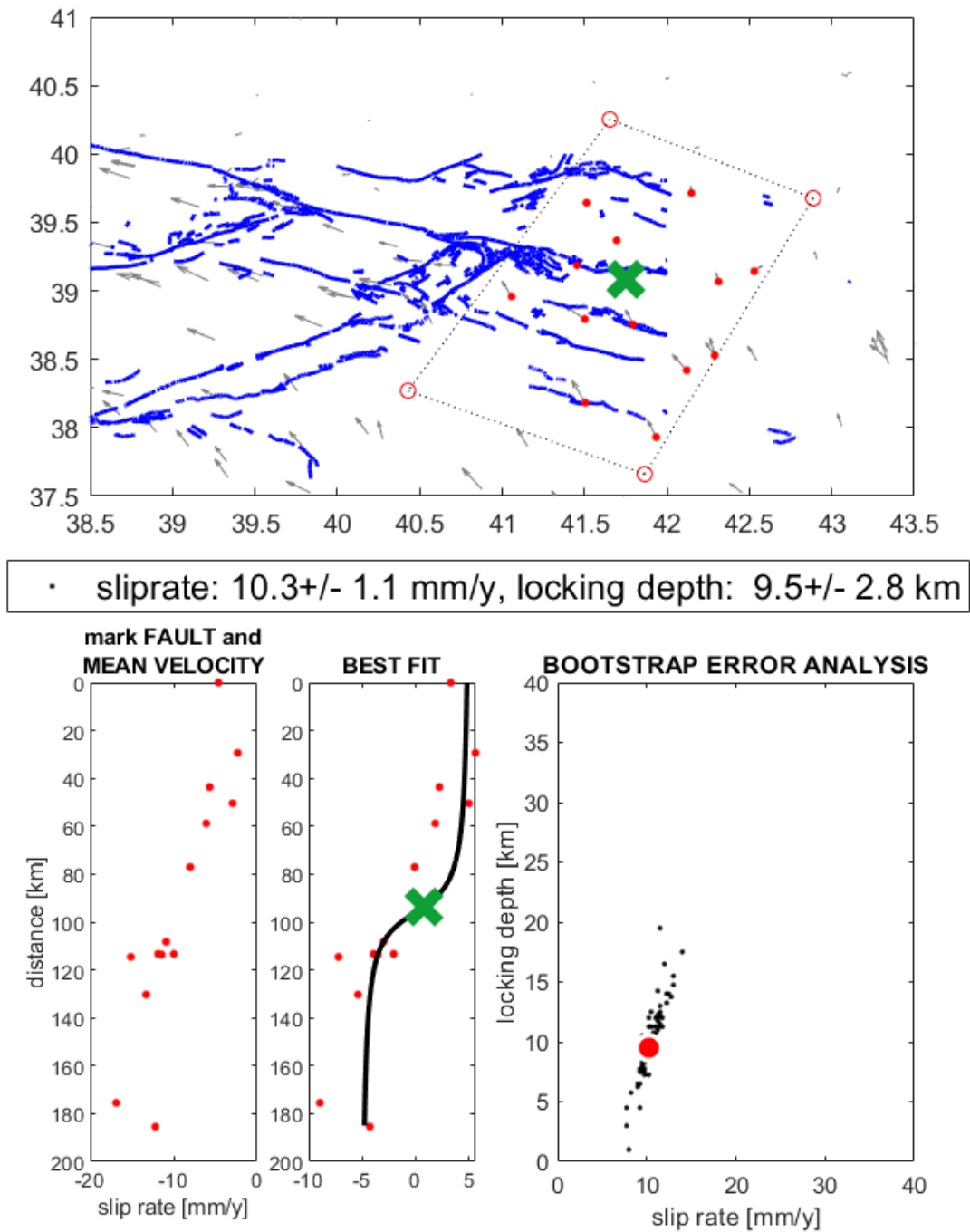


Figure 4.1.2. Arctangent analysis of the possible southeast extension of the NAF section. In the upper panel, the location of the marked fault used for the best fit solution is shown with a green “X” marker in the lower panel, and the region where the profile was taken.

In the section of the possible eastern extension of the NAF, reference frame was fixed in the north of fault, and profile perpendicular to the fault was taken approximately 200 km

long. Marked mean velocity and fault location are shown with green “X” marker (Figure 4.1.3). The slip rate was found to be 6.8 mm/year with an error margin of 0.4 mm/year, and the locking depth as 18.0 km with an error margin of 2.8 km.

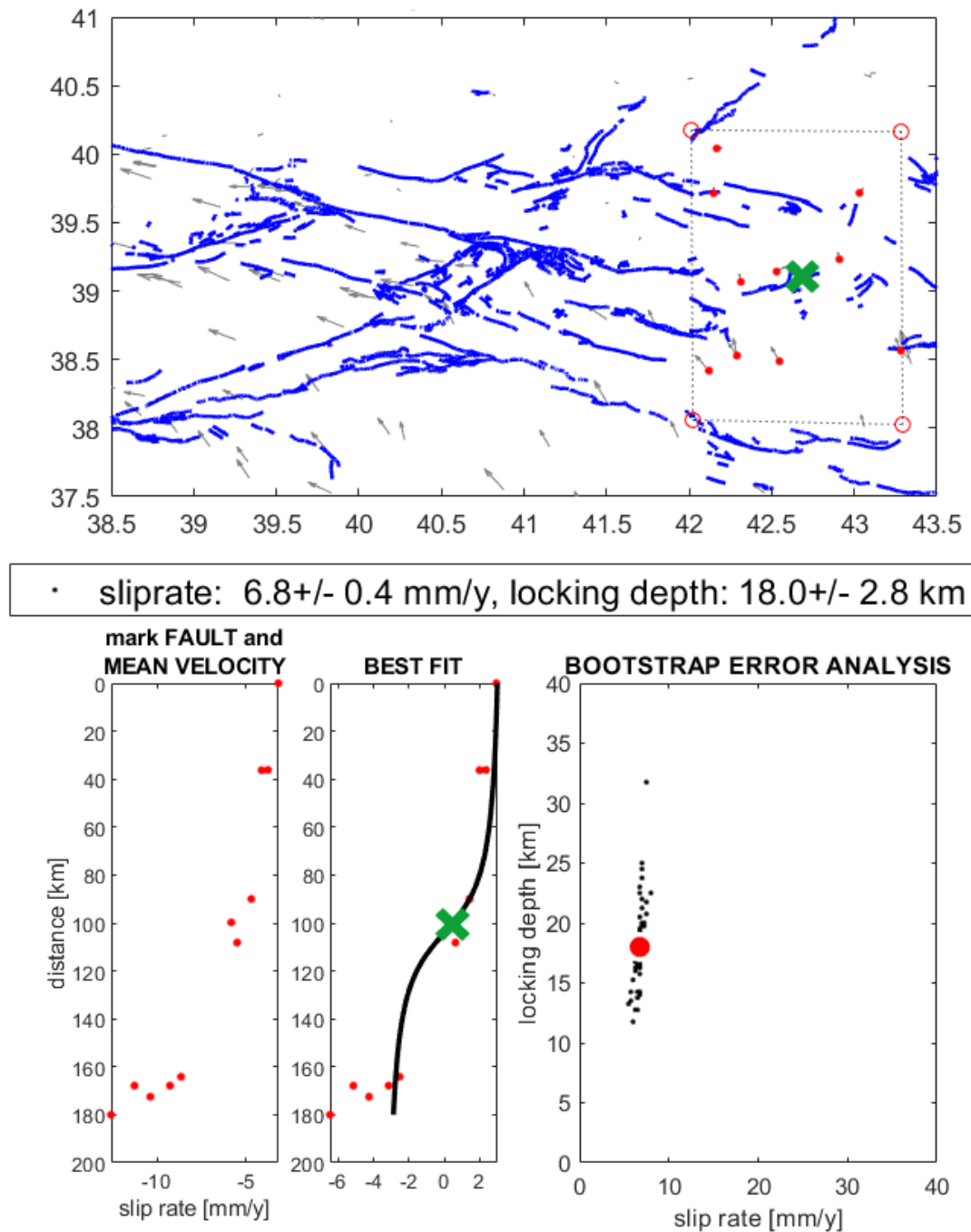


Figure 4.1.3. Arctangent analysis of the possible eastern extension of the NAF section. In the upper panel, the location of the marked fault used for the best fit solution is shown with a green “X” marker in the lower panel, and the region where the profile was taken.

In the section of the EAF, reference frame was fixed in the south of the EAF, and profile perpendicular to the fault was taken approximately 230 km long. Marked mean velocity and fault location are shown with green “X” marker in the Figure 4.1.4. The slip rate was found to be 10.5 mm/year with an error margin of 0.6 mm/year, and the locking depth as 15.3 km with an error margin of 4.6 km.

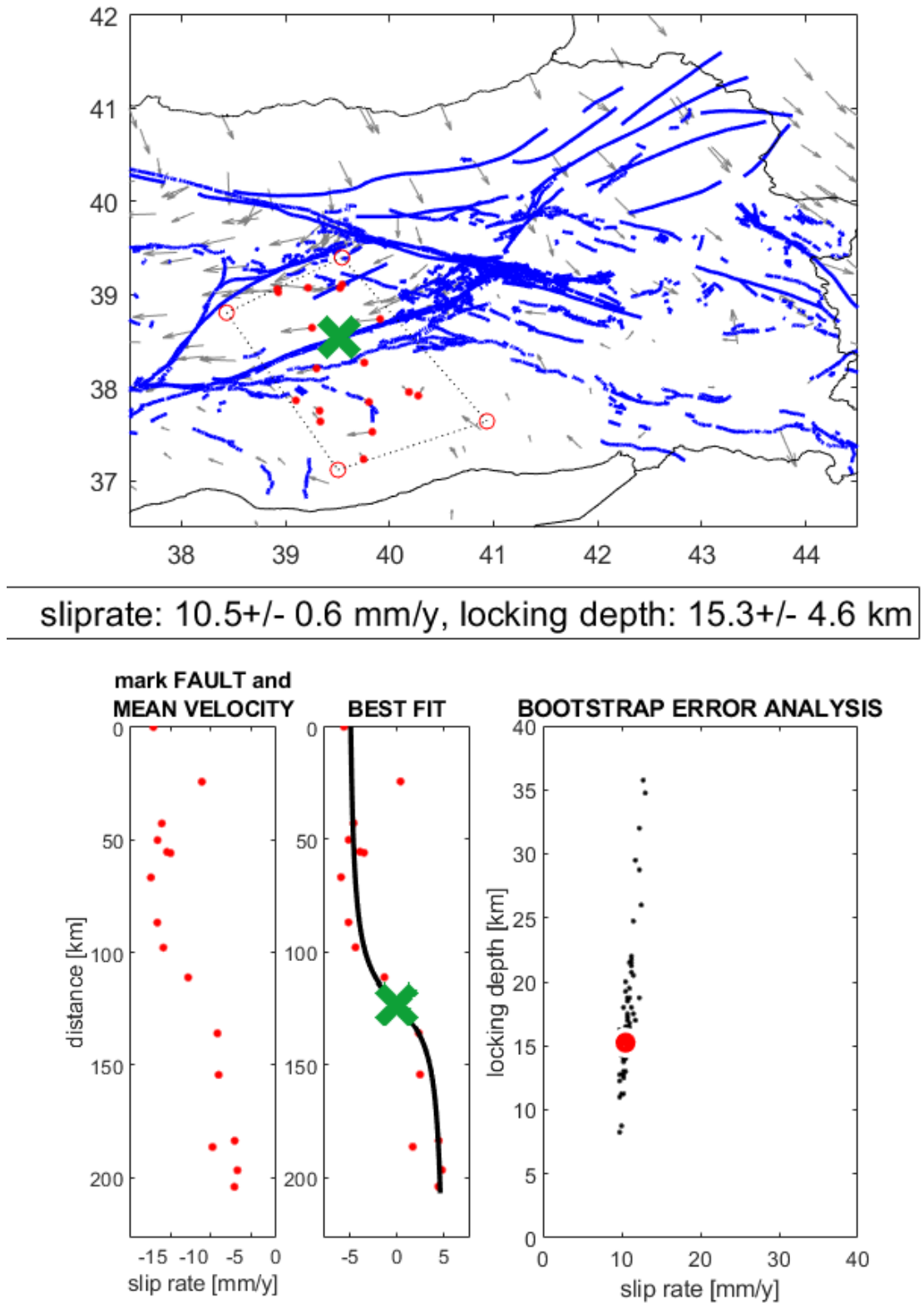


Figure 4.1.4. Arctangent analysis of the EAF section. In the upper panel, the location of the marked fault used for the best fit solution is shown with a green “X” marker in the lower panel, and the region where the profile was taken.

In the section of the possible northeastern extension of the EAF, reference frame was fixed is the southeast of the fault, and profile perpendicular to the fault was taken approximately 125 km long. Marked mean velocity and fault location are shown with green “X” marker (Figure 4.1.5). The slip rate was found to be 5.8 mm/year with an error margin of 1.0 mm/year, and the locking depth as 13.5 km with an error margin of 6.5 km.

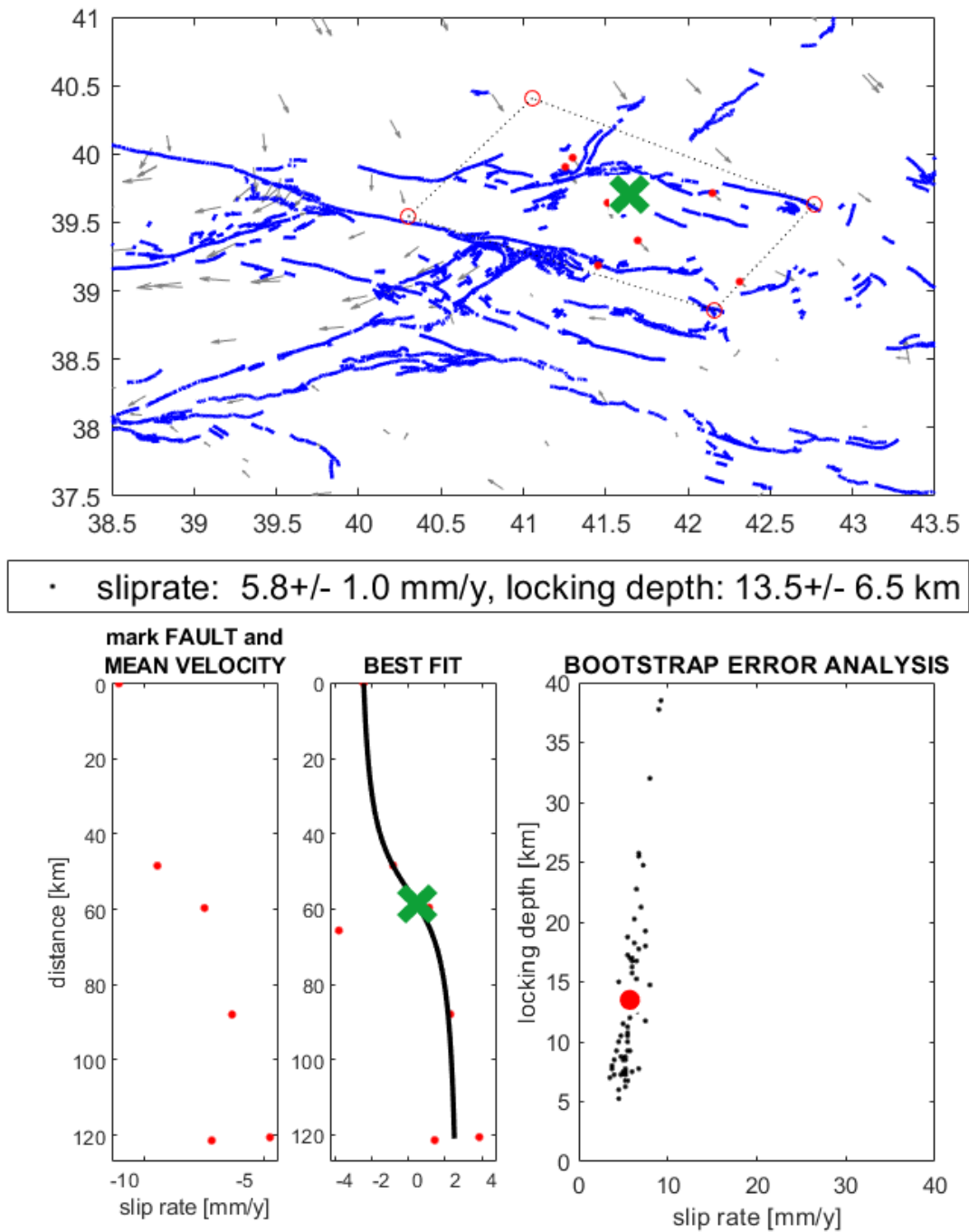


Figure 4.1.5. Arc tangent analysis of the possible northeastern extension of the EAF section. In the upper panel, the location of the marked fault used for the best fit solution is shown with a green “X” marker in the lower panel, and the region where the profile was taken.

Table 4.1. Slip rates and locking depths from arctangent analysis. Abbreviations, SR, LD mean slip rate and locking depth, respectively.

Segments	Slip Rate (mm/y)	Error Margin of SR (mm/y)	Locking Depth (km)	Error Margin of LD (km)
The NAF section	19.8	0.8	19.3	1.7
Possible southeast extension of the NAF	10.3	1.1	9.5	2.8
Possible eastern extension of the NAF	6.8	0.4	18.0	2.8
The EAF section	10.5	0.6	15.3	4.6
Possible northeastern extension of the EAF	5.8	1.0	13.5	6.5

4.2. Block Modeling

The block modeling approach, in which the blocks surrounded by the faults are considered to be rigid, has been used to simultaneously constrain the deformation on all defined fault lines, considering the fault locations that are initially analyzed using the arctangent profiles. ERBLOM (Elastic Rigid BLOck Modeling) software was used where elastic strain along the block boundaries is calculated using analytical equations given by Okada (1985) (Aktug et al., 2013). The GPS velocities that are homogenously compiled from Kremer et al. (2014), Aktug et al. (2016) and Ozdemir (2016) were used as velocity input data. At this stage, 5 blocks (closed polygons) were defined within the study area (Figure 4.2).

As a result of this analysis, the generated values are given in Table 4.2. In the Figure 4.2, upper values are strike slip components and lower values are fault-perpendicular slip rates. The positive values of lateral slip rates indicate the left lateral movement of the fault, while the negative ones indicate the right lateral movement. The positive polarity of the fault-perpendicular slip rates represent shortening, the negative polarity represents extension.

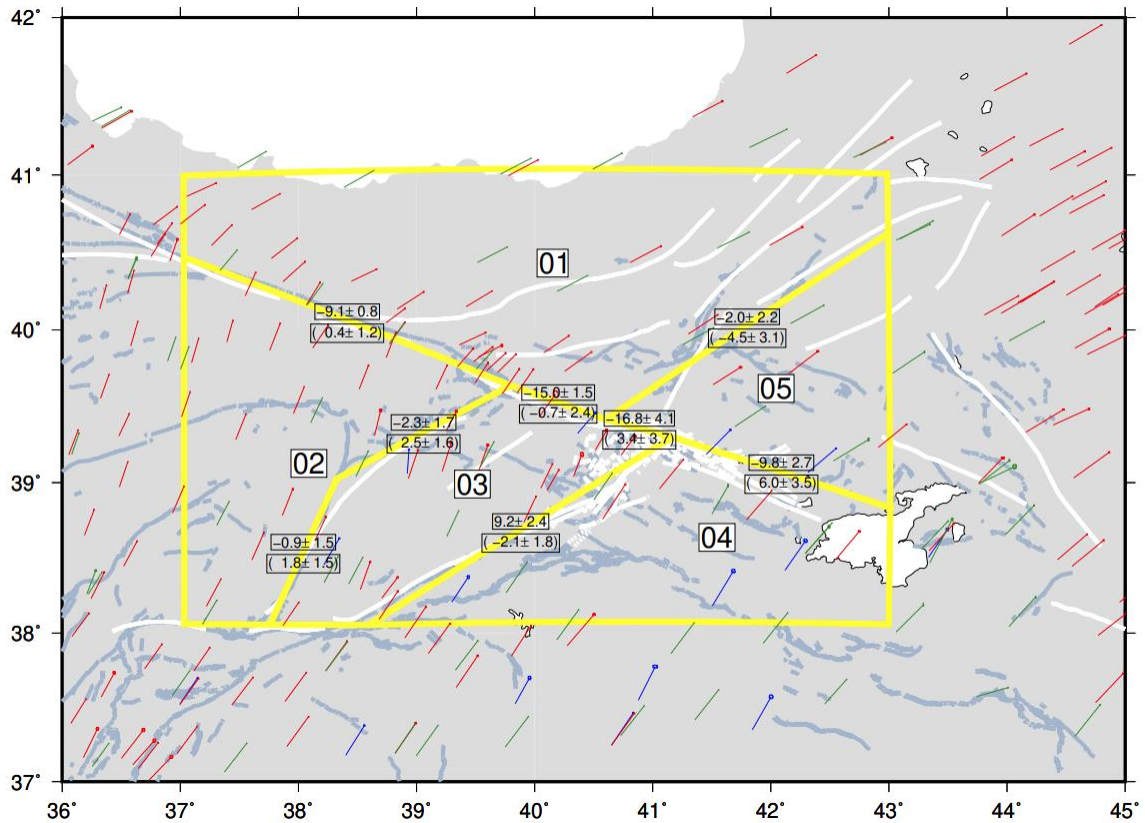


Figure 4.2. Block modeling analysis of the study and the block boundaries indicated with the yellow lines. The faded lines were taken from the MTA, and the white colored faults were taken from previous studies. GPS velocity vectors represent the red ones from Kreemer et al. (2014), the blue ones from Aktug et al. (2016), and the green ones from Ozdemir (2016).

Table 4.2. Slip rates from block modeling analysis.

Blocks	Lateral		Fault-perpendicular	
	Slip Rate (mm/y)	Error Margin (mm/y)	Slip Rate (mm/y)	Error Margin (mm/y)
1 - 2	-9.1	0.8	0.4	1.2
1 - 3	-15.0	1.5	-0.7	2.4
1 - 5	-2.0	2.2	-4.5	3.1
2 - 3	-2.3	1.7	2.5	1.6
2 - 3	-0.9	1.5	1.8	1.5
3 - 4	9.2	2.4	-2.1	1.8
3 - 5	-16.8	4.1	3.4	3.7
4 - 5	-9.8	2.7	6.0	3.5

5. DISCUSSION

The NAF is an arc-shaped dextral strike-slip fault (Bozkurt, 2001). It has many sub-parallel fault strands, and in the east, it merges with the southwest-northeast trending sinistral strike-slip fault EAF (Allen, 1969; Arpat and Saroglu 1972; Barka and Kadinsky-Cade, 1988) at Karlioiva junction. This causes an extensive and complex deformation in the vicinity of Karlioiva. Although, in some studies, the NAF is not terminated at the Karlioiva junction and continues to the southeast, the extensions of the NAF and the EAF were not yet clearly observed. In the instrumental period, there were some major earthquakes along the possible extension of the NAF, such as 1966 Mus-Cayiryolu earthquake (M 6.5), 1982 Erzurum-Hinis earthquake (M 5.4), and 2013 Mus-Suduragi earthquake (M 5.1) (KOERI). Similarly, there were some major earthquakes along the possible extension of the EAF, such as 1983 Kars-Sarikamis earthquake (M 6.8), 1999 Erzurum-Horasan earthquake (M 5.5) and 2013 Erzurum-Tekman earthquake (M 4.5) (KOERI). Also, the last major earthquake on the EAF is 2020 Elazığ earthquake (M 6.75) (Dogru et al., 2021). These earthquakes, and similar major earthquakes in historical earthquake catalog represent a first line of evidence for continuation of the NAF and the EAF in the east of Karlioiva.

In the frame of this study, possible extensions of the NAF and EAF to the east beyond Karlioiva were investigated using locations and mechanisms of earthquakes, and arctangent modeling of GPS measurements. The region of interest is selected to cover a broad area large enough to characterize the faults, the intersection area (Karlioiva junction), and eastern Turkey. Interseismic period GPS velocities were used as the main data source. Besides, the locations of tectonic structures detected in previous studies were investigated. By using these data, two different analyzes were performed, namely arctangent profiling and block modeling, in order to detect the presence of possible extensions. As expected, results depend on the number of GPS velocities in the area and the selection of the blocks.

The arctangent modeling proposed by Savage and Burford (1973), which is implemented by Bulut and Dogru (2021), allows obtaining the slip rates and locking depths at different fault segments in the region of interest. In this study, the position of possible extensions, their slip rates, and locking depths were investigated. For the NAF section, the

slip rate was found to be 19.8 ± 0.8 mm/y. This is in good correspondence with the previous observations, e.g., by Aktug et al. (2015), where the slip rate of the easternmost segment of the NAF is reported to be 19.8 ± 2.3 mm/y, by Cakir et al. (2014) where the slip rate of this segment of the NAF is reported to be 20 ± 3 mm/y, and by Tatar et al. (2012), where the slip rate of this segment of the NAF is reported to be 20.1 ± 2.4 mm/y. The locking depth of the NAF section found to be 19.3 ± 1.7 km which is compatible with Walters et al. (2011) that argued the locking depth of the eastern NAF is between 13.5 - 25 km, however; Aktug et al. (2015) stated the locking depth of the easternmost NAF is 11.9 ± 3.5 km and Tatar et al. (2012) mentioned the locking depth of the NAF is 12.5 ± 3.5 km. Along the possible southeast extension of the NAF section, it is seen that the slip rate decreases by half to the east with respect to the slip rate in the northwest.

As a result of the arctangent analysis in the EAF section, slip rate is 10.5 ± 0.6 mm/y, and the locking depth is 15.3 ± 4.6 km. It is also compatible with Aktug et al. (2016) that mentioned that the slip rate of the northern EAF is 11.06 ± 3.94 mm/y, and the locking depth is 28.85 ± 29.24 km. Further, in the possible northeastern extension of the EAF section, the slip rate is reduced by half in the same way and the presence of extensions continues.

For block modeling analysis, all fault traces in the region of interest have been merged and simplified to define block boundaries. We finally defined five blocks. Since the blocks are analyzed as a single rigid part in block modeling, slips detected at the block boundaries indicate a movement at these boundaries. The corresponding block boundaries on the NAF in three sections (the boundaries between blocks 1-2, 1-3, 3-5), the average right lateral slip rate is about 13.6 mm/y. The boundary, between blocks 4 and 5, representing the extension of the NAF, has a right lateral slip velocity of about 9.8 ± 2.7 mm/y, which is compatible with Reilinger et al. (2006) arguing the slip rate of this block boundary is 11.9 ± 0.4 mm/y. Ahadov and Jin (2021) stated that the slip rate of this boundary ranges between 10 - 12 mm/y. In the boundary, between blocks 3 and 4, that overlaps with the EAF, the slip rate is ~ 9.2 mm/y, left lateral. The slip rate of the boundary, between blocks 1 and 5, which is the continuation of the EAF to the northeast, is about 2.2 mm/y. This is consistent with Reilinger et al. (2006) arguing that the slip rate of this block boundary is 2.3 ± 0.2 mm/y. Ahadov and Jin (2021) reported that the slip rate of this boundary range between 2 - 4 mm/y. On the contrary, Aktug et al. (2013) found that the slip rate of this boundary is 4.7 ± 0.3

mm/y. The blocks in the studies of Aktug et al. (2013), Reilinger et al. (2006) and Ahadov and Jin (2021), which are within the region of interest of this study, cover approximately a similar area.

The results of the arctangent analysis are consistent with previous studies. In the block modeling analysis, calculations are made using only the velocity field inside the blocks (Cakmak, 2011), that is, slip rates of the two blocks relative to each other were obtained. For this reason, the slip rates obtained from arctan modeling are mainly verified the results of block modeling analysis.

6. CONCLUSIONS

(i) Historical earthquakes for almost the last two millennia as well as the instrumental period earthquakes (since 1900) are localized along the NAF and the EAF in the west of Karlioiva junction.

(ii) Instrumental period earthquakes indicate an epicentral distribution of the NAF remain as it is in the southeast of Karlioiva, suggesting that the NAF continue with the same local strike, which is NW-SE, to the southeast of Karlioiva, towards the Van Lake.

(iii) Instrumental period earthquakes do not provide a clear evidence for the continuation of the EAF, as they indicate a seismic activity along rather a broad region in the northeast of Karlioiva.

(iv) Fault plane solutions verify dextral characteristic of the NAF in the northwest of Karlioiva. They remain as they are also beyond Karlioiva confirming a dextral continuation of the NAF to the southwest.

(v) Fault plane solutions indicate sinistral characteristic of the EAF in the southwest of Karlioiva. Towards the northeast of Karlioiva, left-lateral mechanisms are available for NE-SW striking nodal planes. However, they are distributed to a broad area, which do not provide a clear evidence for northeastern continuation of the EAF beyond Karlioiva.

(vi) The NAF deforms at 19.8 mm/y slip rate down to 19.3 km locking depth in the northwest of Karlioiva.

(vii) The EAF deforms at 10.5 mm/y slip rate down to 15.3 km locking depth in the southwest of Karlioiva.

(viii) In the southeast of Karlova, an arctangent profile indicates a dextral fault deforming at 10.3 mm/y slip rate down to 9.5 km locking depth with the similar strike suggesting that the NAF extends towards the southeast of Karlova for ~170 km with a similar fault kinematics but almost half a deformation rate.

(ix) In the northeast of Karlova, an arctangent profile indicates a sinistral fault deforming at 5.8 mm/y slip rate down to 13.5 km locking depth with a similar strike suggesting that the EAF extends towards the northeast of Karlova for ~180 km with a similar fault kinematics but almost half a deformation rate.

Future works require a denser GPS network in the region to better resolve the slip rates of the main faults and their extensions. In order to define the role of these extensions in earthquake hazards of the region, geological fieldworks needs to be increased.

REFERENCES

- Ahadov, B., and S., Jin., 2021, “Slip Rates and Seismic Potential Along Main Faults in the Eastern Mediterranean and Caucasus from Dense GPS Observations and Seismic Data.”, *Pure and Applied Geophysics*, Vol. 178, No. 1, pp. 39–54.
- Aktug, B., A. Dogru, H. Ozener, and M. Peyret, 2015, “Slip rates and locking depth variation along central and easternmost segments of North Anatolian Fault”, *Geophysical Journal International*, Vol. 202, No. 3, pp. 2133–2149.
- Aktuğ, B., H. Ozener, A. Dogru, A. Sabuncu, B. Turgut, K. Halicioglu, O. Yilmaz, and E. Havazli, 2016, “Slip rates and seismic potential on the East Anatolian Fault System using an improved GPS velocity field.”, *Journal of Geodynamics*, Vol. 94-95, pp. 1–12.
- Aktug, B., U., Dikmen, A., Dogru, H., Ozener, 2013, “Seismicity and strain accumulation around Karlioiva Triple Junction (Turkey).”, *Journal of Geodynamics*, Vol. 67, pp. 21–29.
- Aktug, B., U. Dikmen, A. Dogru, and H. Ozener, 2013, “Seismicity and strain accumulation around Karlioiva Triple Junction (Turkey).”, *Journal of Geodynamics*, Vol. 67, pp. 21–29.
- Allen, C. R., 1969, “Active faulting in northern Turkey”, *Division of Geological Science, Calif. Inst. Technol. Contrib.*, 1577, 32.
- Ambraseys, N. N. and J. A. Jackson, 1998, “Faulting associated with historical and recent earthquakes in the Eastern Mediterranean region.”, *Geophysical Journal International*, Vol. 133, No. 2, pp. 390–406.
- Arpat, E. and F. Şaroğlu, 1972, "The East Anatolian Fault System; Thoughts on its Development", *Bulletin of the Mineral Research and Exploration*, Vol. 78, No. 78, pp. 1-12.

- Barka, A. A., and K. Kadinsky-Cade, 1988, “Strike-Slip Fault Geometry in Turkey and Its Influence on Earthquake Activity.”, *Tectonics*, Vol. 7, No. 3, pp. 663–684.
- Bohnhoff, M., P. Martínez-Garzón, F. Bulut, E. Stierle, and Y. Ben-Zion, 2016, “Maximum earthquake magnitudes along different sections of the North Anatolian fault zone.”, *Tectonophysics*, Vol. 674, pp. 147–165.
- Bozkurt, E., 2001, “Neotectonics of Turkey – a Synthesis.”, *Geodinamica Acta*, Vol. 14, No. 1-3, pp. 3–30.
- Bulut, F., and A. Doğru, 2021, “Time Frame for Future Large Earthquakes near İstanbul Based on East-to-West Decelerating Failure of the North Anatolian Fault”, *TURKISH JOURNAL OF EARTH SCIENCES*, Vol. 30, No. 2, pp. 204–214.,
- Bulut, F., M. Bohnhoff, T. Eken, C. Janssen, T. Kılıç, and G. Dresen, 2012, “The East Anatolian Fault Zone: Seismotectonic setting and spatiotemporal characteristics of seismicity based on precise earthquake locations”, *Journal of Geophysical Research: Solid Earth*, Vol. 117, No. B7, 2012.
- Cakir, Z., S., Ergintav, A. M., Akoğlu, R., Çakmak, O., Tatar, M., Meghraoui, 2014, “InSAR velocity field across the North Anatolian Fault (eastern Turkey): Implications for the loading and release of interseismic strain accumulation”, *Journal of Geophysical Research: Solid Earth*, Vol. 119, No. 10, pp. 7934–7943.
- Cakmak, R., 2011, *Jeodezik çalışmalarla Marmara Bölgesinde deprem döngüsünün belirlenmesi ve modellerle açıklanması*, PhD, Istanbul Technical University Institute of Science and Technology.
- Doğru, A., F. Bulut, C. Yalıtırak, B. Aktuğ, 2021, “Slip distribution of the 2020 Elazığ Earthquake (M w 6.75) and its influence on earthquake hazard in the Eastern Anatolia.”, *Geophysical Journal International*, Vol.224, No.1, pp. 389-400.
- Emre, Ö., T. Y. Duman, S. Özalp, F. Şaroğlu, Ş. Olgun, H. Elmacı, and T. Çan, 2018, “Active fault database of Turkey”, *Bulletin of Earthquake Engineering*, Vol. 16, No. 8, pp. 3229–3275.

- İmamoğlu, M. and E. Çetin, 2007, “Güneydoğu Anadolu Bölgesi ve Yakın Yöresinin Depremselliği”, *Dicle Üniversitesi Ziya Gökalp Eğitim Fakültesi Dergisi*, No. 9, pp. 93-103.
- ISC, *International Seismological Centre, ISC Bulletin: Focal mechanism search*, 2021, <http://www.isc.ac.uk/iscbulletin/search/fmechanisms/>.
- Karakhanian, A. S., V. G. Trifonov, H. Philip, A. Avagyan, K. Hessami, F. Jamali, M. Salih Bayraktutan, H. Bagdassarian, S. Arakelian, V. Davtian, and A. Adilkhanyan, 2004, “Active faulting and natural hazards in Armenia, eastern Turkey and northwestern Iran”, *Tectonophysics*, Vol. 380, No. 3-4, pp. 189–219.
- KOERI, *Boğaziçi University Kandilli Observatory Earthquake Research Institute, BDTIM Earthquake Query System*, 2021, <http://www.koeri.boun.edu.tr/sismo/>.
- Kreemer, C., G. Blewitt, and E. C. Klein, 2014, “A geodetic plate motion and Global Strain Rate Model”, *Geochemistry, Geophysics, Geosystems*, Vol. 15, No. 10, pp. 3849–3889.
- McKenzie, D., 1976, “The East Anatolian Fault: A major structure in Eastern Turkey”, *Earth and Planetary Science Letters*, Vol. 29, No. 1, pp. 189–193.
- McKenzie, D. and N. Weiss, 2007, “Speculations on the Thermal and Tectonic History of the Earth”, *Geophysical Journal of the Royal Astronomical Society*, Vol. 42, No. 1, pp. 131–174.
- McClusky, S., S. Balassanian, A. Barka, C. Demir, S. Ergintav, I. Georgiev, I. G. Veis, 2000, “Global Positioning System constraints on plate kinematics and dynamics in the eastern Mediterranean and Caucasus.”, *Journal of Geophysical Research: Solid Earth*, Vol. 105 No. B3, pp. 5695-5719.
- MTA, *General Directorate of Mineral Research and Exploration, Active Fault Map of Turkey*, 2020, <https://www.mta.gov.tr/v3.0/hizmetler/yenilenmis-diri-fay-haritalari>
- Muehlberger, W. R. and M. B. Gordon, 1987, “Observations on the complexity of the east anatolian fault, Turkey”, *Journal of Structural Geology*, Vol. 9, No. 7, pp. 899–903.

- Okada, Y., 1985, "Surface deformation due to shear and tensile faults in a half-space", *Bulletin of the seismological society of America*, Vol. 75, No .4, pp. 1135-1154.
- Ozdemir, S., 2016, "On the estimation of precise coordinates and velocities of TNPGN and TNPGN-active stations", *Harita Dergisi*, Vol. 155, pp. 53-81.
- Perinçek, D., Y. Günay, and H. Kozlu, 1987, "Doğu ve Güneydoğu Anadolu Bölgesi'ndeki yanal atımlı faylar ile ilgili yeni gözlemler", *Türkiye 7th Petrol Kongreleri Bildirileri*, 89-104.
- Philip, H., A. Avagyan, A. Karakhanian, J.-F. Ritz, and S. Rebai, 2001, "Estimating slip rates and recurrence intervals for strong earthquakes along an intracontinental fault: example of the Pambak–Sevan–Sunik fault (Armenia)", *Tectonophysics*, Vol. 343, No. 3-4, pp. 205–232, 2001.
- Philip, H., A. Cisternas, A. Gvishiani, and A. Gorshkov, 1989, "The Caucasus: an actual example of the initial stages of continental collision", *Tectonophysics*, Vol. 161, No. 1-2, pp. 1–21.
- Rebai, S., H. Philip, L. Dorbath, B. Borissoff, H. Haessler, and A. Cisternas, 1993, "Active tectonics in the Lesser Caucasus: Coexistence of compressive and extensional structures", *Tectonics*, Vol. 12, No. 5, pp. 1089–1114.
- Reilinger, R., S., McClusky, P., Vernant, S., Lawrence, S., Ergintav, R., Cakmak, H., Ozener, F., Kadirov, I., Guliev, R., Stepanyan, M., Nadariya, G., Hahubia, S., Mahmoud, K., Sakr, A., ArRajehi, D., Paradissis, A., Al-Aydrus, M., Prilepin, T., Guseva, G., Karam, 2006, "GPS constraints on continental deformation in the Africa-Arabia-Eurasia continental collision zone and implications for the dynamics of plate interactions.", *Journal of Geophysical Research: Solid Earth*, Vol. 111, No.5.
- Savage, J. C., and R. O. Burford, 1973, "Geodetic Determination of Relative Plate Motion in Central California.", *Journal of Geophysical Research*, Vol.78, No. 5, pp. 832-845.

- Sengör, A. M. C., 1979, "The North Anatolian transform fault: its age, offset and tectonic significance.", *Journal of the Geological Society*, Vol. 136, No. 3, pp. 269-282.
- Şengör, A. C., N. Canitez, 1982, "The North Anatolian Fault.", *Alpine-Mediterranean Geodynamics*, Vol.7, pp. 205-216.
- Şengör, A. M., N. Görür, and F. Şaroğlu, 1985, "Strike-Slip Faulting and Related Basin Formation in Zones of Tectonic Escape: Turkey as a case study", *Strike-Slip Deformation, Basin Formation, and Sedimentation*, pp. 227–264.
- Tatar, O., F., Poyraz, H., Gürsoy, Z., Cakir, S., Ergintav, Z., Akpınar, H., Yavaşoğlu, 2012, "Crustal deformation and kinematics of the eastern part of the North Anatolian fault ZONE (turkey) from GPS measurements", *Tectonophysics*, Vol. 518-521, pp. 55-62.
- Taymaz, T., J. Jackson, and R. Westaway, 1990, "Earthquake mechanisms in the Hellenic Trench near Crete", *Geophysical Journal International*, Vol. 102, No. 3, pp. 695-731.
- Taymaz, T., H. Eyidoğan, J. Jackson, 1991, "Source parameters of large earthquakes in the East Anatolian Fault Zone (Turkey).", *Geophysical Journal International*, Vol. 106, No. 3, pp. 537-550.
- Walters, R. J., R. J., Holley, B., Parsons, T. J., Wright, 2011, "Interseismic strain accumulation across the North Anatolian Fault from Envisat InSAR measurements", *Geophysical Research Letters*, Vol. 38, No. 5.